Article

Mechanistic Insight for Targeting Biomolecules by Ruthenium(II) NSAID Complexes

Chanchal Sonkar, Novina Malviya, Rishi Ranjan, Srimanta Pakhira, and Suman Mukhopadhyay

ACS Appl. Bio Mater., **Just Accepted Manuscript** • DOI: 10.1021/acsabm.0c00501 • Publication Date (Web): 22 Jun 2020

Mechanistic Insight for Targeting Biomolecules by Ruthenium(II) NSAID Complexes

Chanchal Sonkar[b], Novina Malviya[a], Rishi Ranjan[a], Srimanta Pakhira[c,d] and Suman Mukhopadhyay[a,b*]

[a]Discipline of Chemistry, School of Basic Sciences, Indian Institute of Technology Indore, Khandwa Road, Simrol, Indore 453552, India

[b]Discipline of Biosciences and Biomedical Engineering, School of Engineering, Indian Institute of Technology Indore, Khandwa Road, Simrol, Indore 453552, India

[c]Discipline of Physics, School of Basic Sciences, Indian Institute of Technology Indore, Khandwa Road, Simrol, Indore 453552, India.

[d]Discipline of Metallurgy Engineering and Materials Science (MEMS), School of Engineering, Indian Institute of Technology Indore, Khandwa Road, Simrol, Indore 453552, India

KEYWORDS: Ruthenium NSAID complexes, biomolecular interactions, Hoechst and Hoechst-PI staining, cell cycle, wound healing, RT-PCR, DFT, B3LYP

ABSTRACT: With enormous progress of ruthenium complexes as promising anticancer agents after the entry of KP1019, KP1339, and NAMI-A in clinical trials, herein three arene ruthenium(II) NSAID (non-steroidal anti-inflammatory drugs) complexes *viz*. [Ru(η^6-*p*-cymene)(mef)Cl] **(1)**, [Ru(η^6-*p*-cymene)(flu)Cl] **(2)**, [Ru(η^6-*p*-cymene)(dif)Cl] **(3)** are synthesized, characterized and reported. Density Functional Theory (DFT) calculations were performed in support of the obtained experimental results by computing the equilibrium geometries, reactions pathways, relative Gibbs free energy, stability, and reactions barriers of the complexes. The present theoretical study shows that all the proposed structures of the complexes are energetically stable and favorable, and the results obtained are in close accordance with the experiment. Further, the *in vitro* cytotoxicity of the complexes was explored through MTT

assay on MCF-7, Hela, A549, and HEK cell lines. It was found the complex **1** and **2** are significantly cytotoxic toward the MCF-7 cell line. These complexes have also shown a strong affinity towards CT-DNA and proteins (HSA and BSA) as analyzed through spectroscopic techniques. Further investigation of the mechanism of cell death of selected complexes was carried out by various staining, flow cytometry, and gene expression analysis obtained by RT-PCR.

INTRODUCTION

With the advent of platinum-based anticancer drugs and their associated side effects, a lot of focus has been given on some alternative metal ions which can bring about a similar result with minimum side effects and can prevail as a potent medicine in realm of cancer chemotherapy[1]. In search of that in the last couple of decades, ruthenium has been emerged as a most promising option as metal ions to fight with cancer as it has shown immense potential to arrest cell cycle progression by interacting with key proteins and enzymes[2]. Some of the ruthenium complexes have also shown anti-angiogenic and anti-metastatic behavior[3]. So it is not a surprise that many ruthenium complexes are being synthesized and tested over the years, and few among them *viz.* NKP-1339, KP1019, and NAMI-A have entered in clinical trial[4]. Among the various other scaffolds which have been tested for anticancer like properties, arene-ruthenium(II) complexes associated with other co-ligands have shown promising activities both *in vitro* and *in vivo*[5]. Insertion of the biologically active ligands within the ruthenium coordination sphere opens up the possibility of combination therapy with a multi-targeted approach. This happens because many a time the ligand with therapeutic value starts to dissociate in biological conditions and both the free ligand and coordinatively unsaturated ruthenium ion can act in tandem as an anti-cancer agent[6].

Discovery of NSAIDs which happened to be a real revolution in the field of medicine is known to target mostly cyclooxygenase enzymes[7] (COX-1 and COX-2) and reduces the production of various prostaglandins responsible for various physiological activities such as fever, pain, and inflammation[8].

Targeting cancerous cells with NSAIDs is a logical approach as cyclooxygenase (COX) and lipooxygenase (LOX) are commonly upregulated in malignant tumors (particularly COX-2)[9]. The COX enzyme's major function is found to be in renal blood flow, the proper function of platelets, and mitogenesis. On the other hand, LOX plays an active role in the formation of hydroxyeicosatetraenoic acids (HETEs) which has a noteworthy role in angiogenic activity by the migration of endothelial cells[10]. Furthermore, these NSAIDs also observe chemopreventive roles because of their activity in the inhibition of functioning of epidermal growth factor (EGF) and overexpression of the tumor suppressor gene[11]. NSAIDs have been also reported for the synergistic activity with anti-tumour drugs[12] and are responsible sometimes for cell death mostly by apoptosis[13]. Altogether it is quite logical to try to combine the efficacy of ruthenium(II) arene scaffold and NSAIDs to find out the outcome in terms of anti-cancer activity as well as COX and LOX inhibition study. There are already few reports where NSAIDs are incorporated in the ruthenium coordination spheres which have shown promising anticancer activities against different cell lines[14]. In this particular report, we have utilized three different NSAIDs as potential ligands to include in the coordination sphere of a ruthenium-arene moiety and explored their anti-proliferative property and anti-metastatic activity. Based on the experiments performed in the report, these three ruthenium NSAIDs complexes have found to show cell cycle arrest which might be the probable cause of apoptosis and also a significant inhibitory effect on migration of cancerous cells. Scheme 1 presents a glimpse of the overall basic effects of the synthesized ruthenium complexes on cancerous cells. A computational study has been performed to analyze the experimental observation by exploring the equilibrium structure of the ruthenium dimer with mefenamic acid, flufenamic acid, diflunisal and their complexes. First-order saddle points (i.e. transitions states (TSs)), change of enthalpy (ΔH) and Gibbs free energy (ΔG) with the respective reaction barriers have been also studied through employing first-principles based DFT method[15] to examine the reaction process.

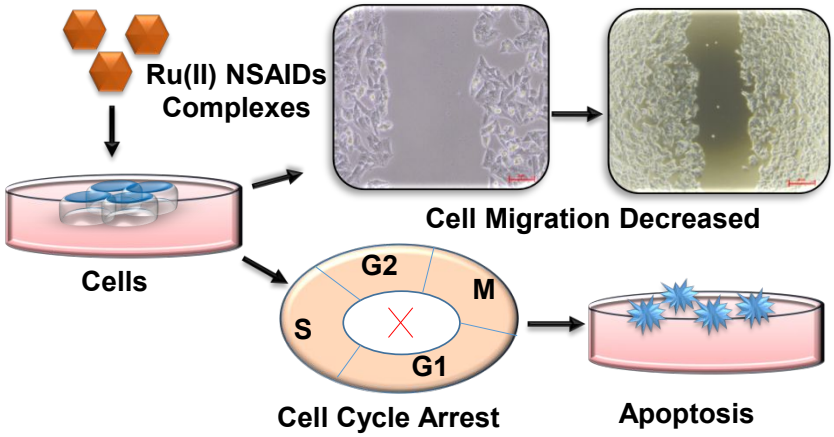

Scheme 1. Graphical depiction of the anticancer property of ruthenium- NSAID complexes (based on the experiments performed in the report).

RESULTS AND DISCUSSION

The complexes **1**, **2**, and **3** were acquired in moderate to good yields by stirring potassium salt solution of NSAID drugs with ruthenium dimer[16,17] $[Ru(\eta^6\text{-}p\text{-cymene})Cl_2]_2$ for overnight in DCM-methanol mixture which was then followed by evaporation to dryness. The mixtures were purified through solubility method, unreacted ligands and reactants were separated from the complexes by extraction with the help of water and DCM. Further, the complexes were recrystallized from a suitable solvent for better purity. The obtained compounds were filtered and washed using hexane and diethyl ether to yield the desired complexes as green powders (Scheme 2). Unfortunately, despite repeated efforts, we were unable to get the single crystals of the isolated complexes to obtain the exact solid-state structure. All three complexes are air-stable, insoluble in water and soluble in DCM, chloroform, methanol, DMF, DMSO. These complexes had been characterized by ESI-MS, IR, elemental analysis, and ^{1}H and ^{13}C NMR. The IR spectra were analyzed carefully to evaluate the possible mode of binding by the carboxylate moiety present in different NSAIDs. The region of the bands for an anti-symmetric and symmetric stretching frequency of carboxylate are found around 1625-1680 cm^{-1} and 1480-1497cm^{-1} respectively. The difference between the asymmetric and symmetric frequencies $\Delta(\nu_{asym}\text{-}\nu_{sym})$ is found to be within the range of 145- 185 cm^{-1} which depicts the bidentate binding mode of carboxylate with the metal ion[18]. Also, there is no significant shift in the IR band of the NH group which reveals the

probable binding of ruthenium with the carboxylate group only and it rules out the possibility of involvement of the NH group in coordination (Figure S1-S3)[19,20]. Furthermore, we have also investigated the binding of ruthenium with the carboxylate group through NMR spectroscopic technique. The ^{1}H spectra of synthesized complexes revealed the *p*-cymene ring protons were within the range of 5.48 to 5.74 ppm and the side-chain protons are observed in the range of 1.40 -1.44, 2.14-2.39 and 2.98-3.00 ppm (Figure 1, S4-S5)[21]. The aromatic protons of the NSAIDs have been observed in the range 6.59-7.88 ppm. Six protons from two methyl groups in the mefenamic complex have shown the signature peaks around 2.32 and 2.38 ppm[22]. Interestingly, we have found the signature peak of NH hydrogen around 8.86 and 9.18 in complex **1** and **2** respectively, which further indicates there is no occurrence of deprotonation that happened for NH- group during coordination as the secondary N stays away from coordination[23]. The ^{13}C spectra of complexes also agree well with the proposed structure (Figure 2, S6-S7). The ^{13}C carbon peaks for the chelating carboxylate have been found in the range of 175-181 ppm indicating their probable behavior as chelating group[24]. This can be also noted herewith that there are already few ruthenium(II)-arene complexes reported which have shown chelating coordination from carboxylate group[25]. The ESI-MS data reveal one major peak envelop indicating $[Ru(\eta^6\text{-}p\text{-cymene})\ (NSAID\text{-}H)]^+$ moiety after the release of the labile chloro ligand in complex **2** and **3** confirming the proposed structures (Figure 3, S8-S9). Whereas in the case of complex **1** the molecular ion peak has been found to corresponds to $[Ru(\eta^6\text{-}p\text{-cymene})(NSAID)Cl + K]^+$. It is worth pointing out here that two mefenamic acetate complexes of ruthenium(II) with arene ring are reported with the molecular formula of $(NH_4)[Ru(\eta^6\text{-}p\text{-cymene})(mef)Cl_2]$ and the ruthenium-benzene analogue[26]. Therefore, to ascertain the composition of the synthesized complexes we have tested the conductance of the complex in DMSO solution, and in each case the conductivity was found to be very less indicating the neutral nature of the synthesized complex in conformity with our proposed structure.

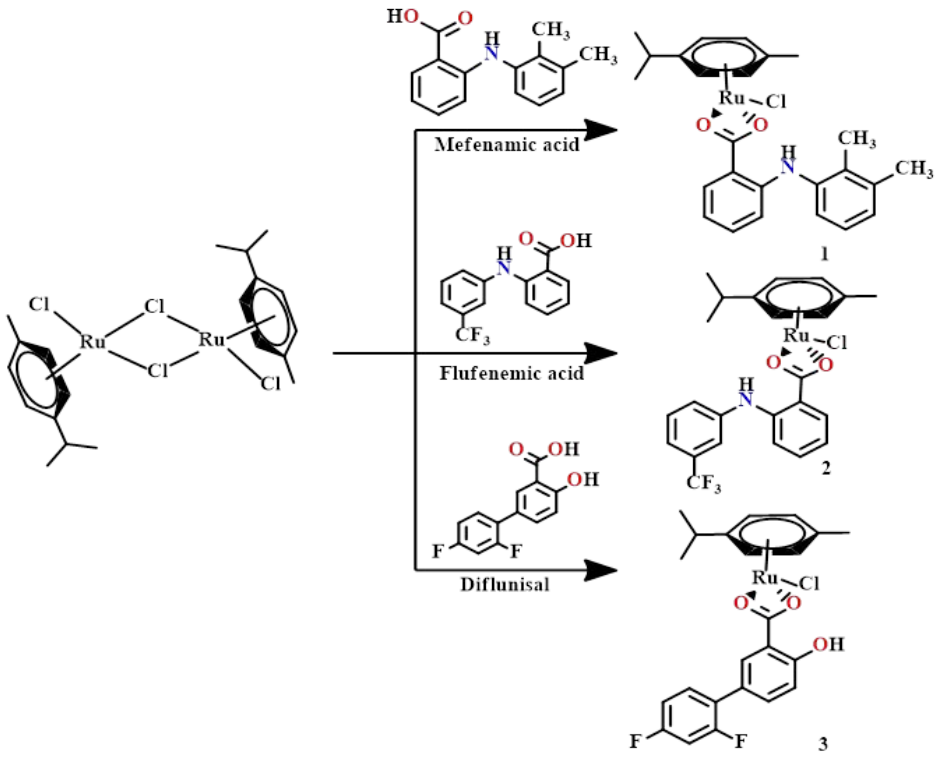

Scheme 2. Schematic diagram of the synthesis of the complex **1**, **2**, **3**.

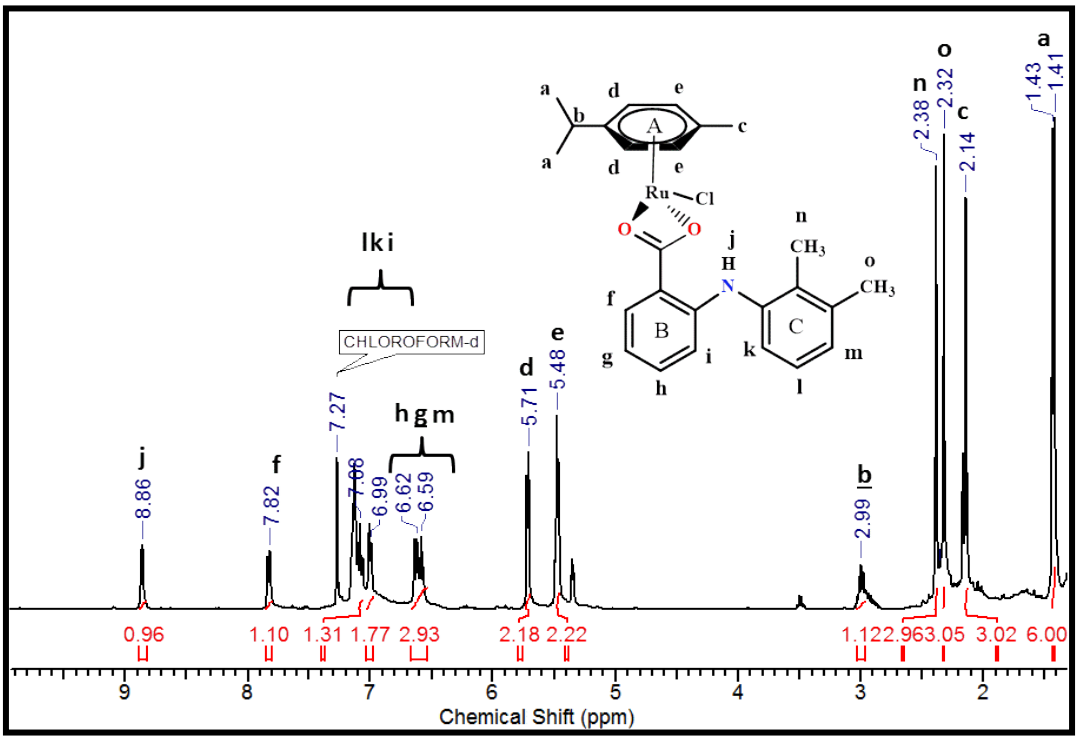

Figure 1: ^{1}H NMR spectra of Complex **1** recorded after dissolving in $CDCl_3$ at room temperature.

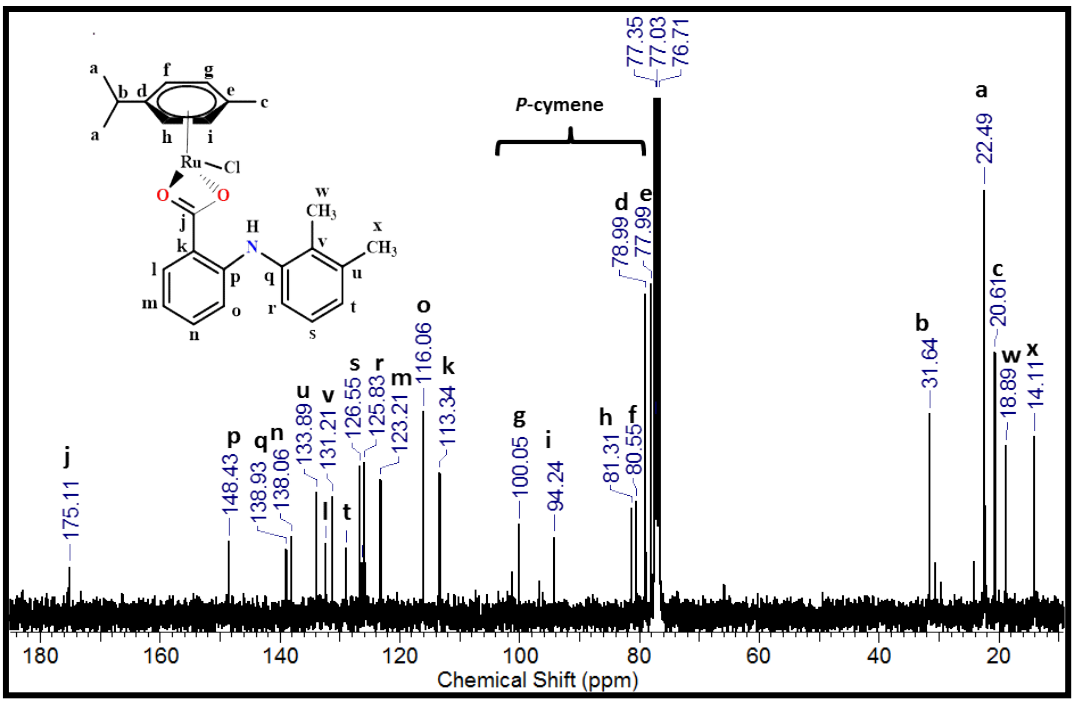

Figure 2: ^{13}C NMR of Complex **1** recorded after dissolving in $CDCl_3$ at room temperature.

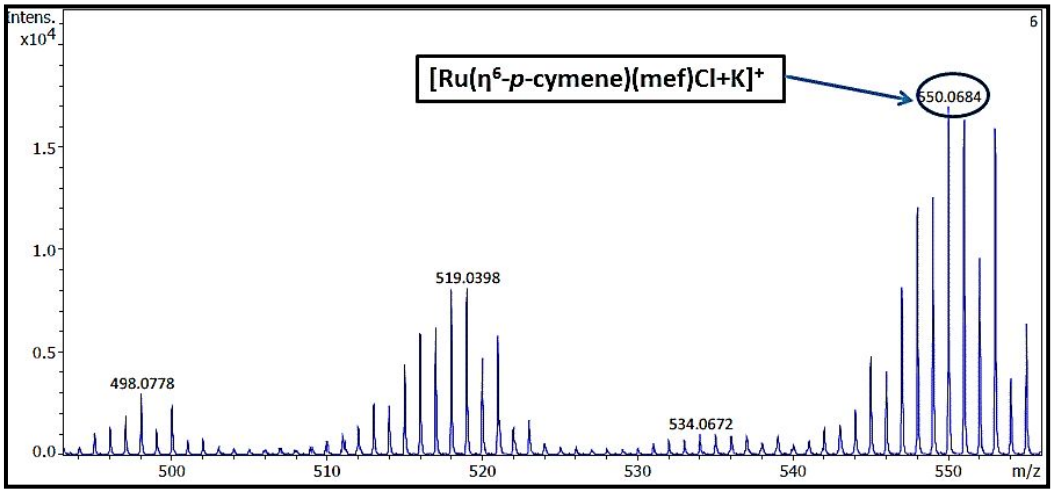

Figure 3. ESI-MS of Complex **1** recorded after dissolving in MeOH at room temperature.

Stability of complexes

For designing new drugs knowing the stability of these complexes in a biological medium plays a crucial role. The ^{1}H and ^{13}C NMR spectra of the synthesized complexes on time-dependent studies show that the complexes are stable throughout twenty-four hours showing no additional peaks or no decrement of the existing peaks indicating the complexes are considerably stable with respect of time in solution (Figure 4, 5 S10-13).

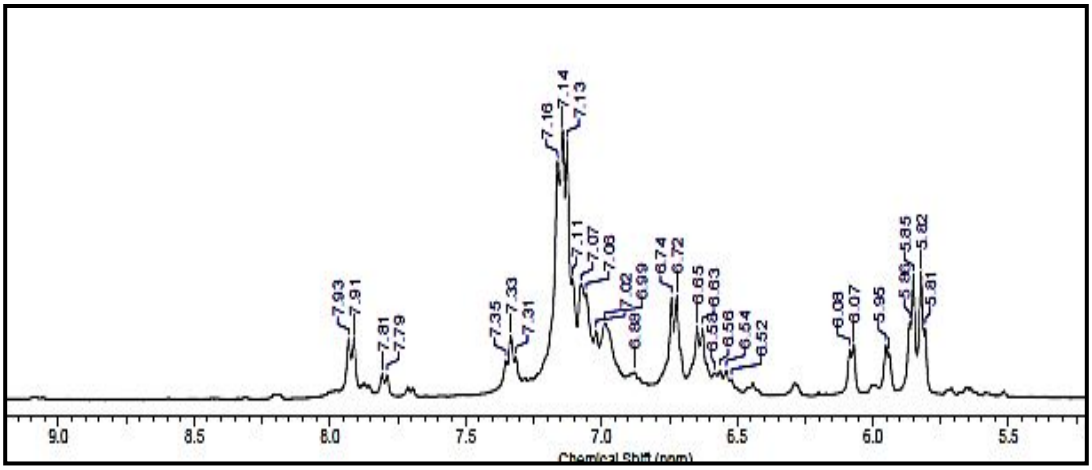

Figure 4. ^{1}H NMR spectra of complex **1** recorded in DMSO-d_6 at 48 h time interval. 10 mg of complex **1** was dissolved in DMSO-d_6 and recorded the spectra at the interval of 0 h, 4 h, 24 h, and 48 h.

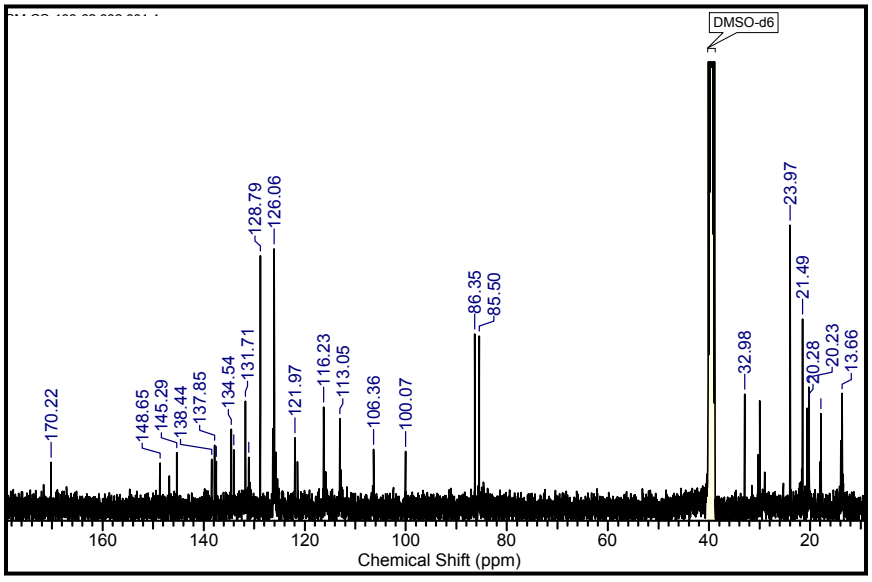

Figure 5. ^{13}C NMR spectra of complex **1** recorded in DMSO-d_6 at 48 h time interval. 10 mg of complex **1** was dissolved in DMSO-d_6 and recorded the spectra at the interval of 0 h, 4 h, 24 h, and 48 h.

Computational studies

DFT calculations have been performed to assist the understanding of three new arene ruthenium(II)-NSAID complexes formation by considering molecular modeling. The equilibrium optimized geometries of the ruthenium dimer, mefenamic acid, flufenamic acid, diflunisal, complex **1**, complex **2**, complex **3**, and transition states (**TS1**, **TS2**, and **TS3**) involved in the reaction were obtained by utilizing the first-principles based B3LYP method, and their structures are shown in Figure 6 (a-j). The present

DFT study determines that all the structures are stable, and the complexes **1**, **2** and **3** formed by a reaction between the ruthenium dimer, and mefenamic acid, flufenamic acid, and diflunisal are energetically stable as shown in Figure 6(e-g), which is well harmonized with our experimental observation. The harmonic vibrational frequency calculations have shown that all the structures and complexes are in stable equilibrium, and it is found that the anti-symmetric and symmetric stretching frequency of the carboxylate in the complexes is around 1685-1744 cm^{-1} and 1475-1505 cm^{-1}, respectively. The computed difference of these anti-symmetric and symmetric stretching frequencies of the same carboxylate in the ruthenium(II)-NSAID complexes $\Delta\nu$ is about in the assortment of 210 - 239 cm^{-1} which is well harmonized with the experiment. The adducts **A1**, **A2**, **A3** are formed by ruthenium dimer, mefenamic acid, flufenamic acid, and diflunisal during the initial reactions. The relative Gibbs free energy i.e. the change of Gibbs free energy (ΔG) has been computed by the same DFT method. The free energy of the transition states (i.e. transition barriers) and the complexes **1**, **2,** and **3** have been computed concerning the adducts **A1**, **A2,** and **A3**, respectively. The change of free energy (ΔG) with the transition barriers of the systems studied here is depicted in Figure 7a-c. It has found that the complex **1** has formed via a transition state **TS1** with a barrier (i.e. ΔG) about 9.68 kcal/mol and the change of enthalpy (ΔH) about 8.69 kcal/mol, and the complex **1** is favorable about an energy -11.40 kcal/mol as shown in Figure 7a. Two transition states **TS2** and **TS3** were found, which links **A2** and complex **2** with a barrier 8.22 kcal/mol, and **A3** and complex **3** with a barrier 13.96 kcal/mol as shown in Figure 7 (b-c). Similarly, complexes **2** and **3** were energetically favorable about -8.91 kcal/mol and -15.45 kcal/mol with the value of ΔH about -8.36 kcal/mol and -13.52 kcal/mol. These calculations reveal that all the complexes: complex **1**, complex **2,** and complex **3** are energetically stable and favorable which are in reasonable accord in our experiment.

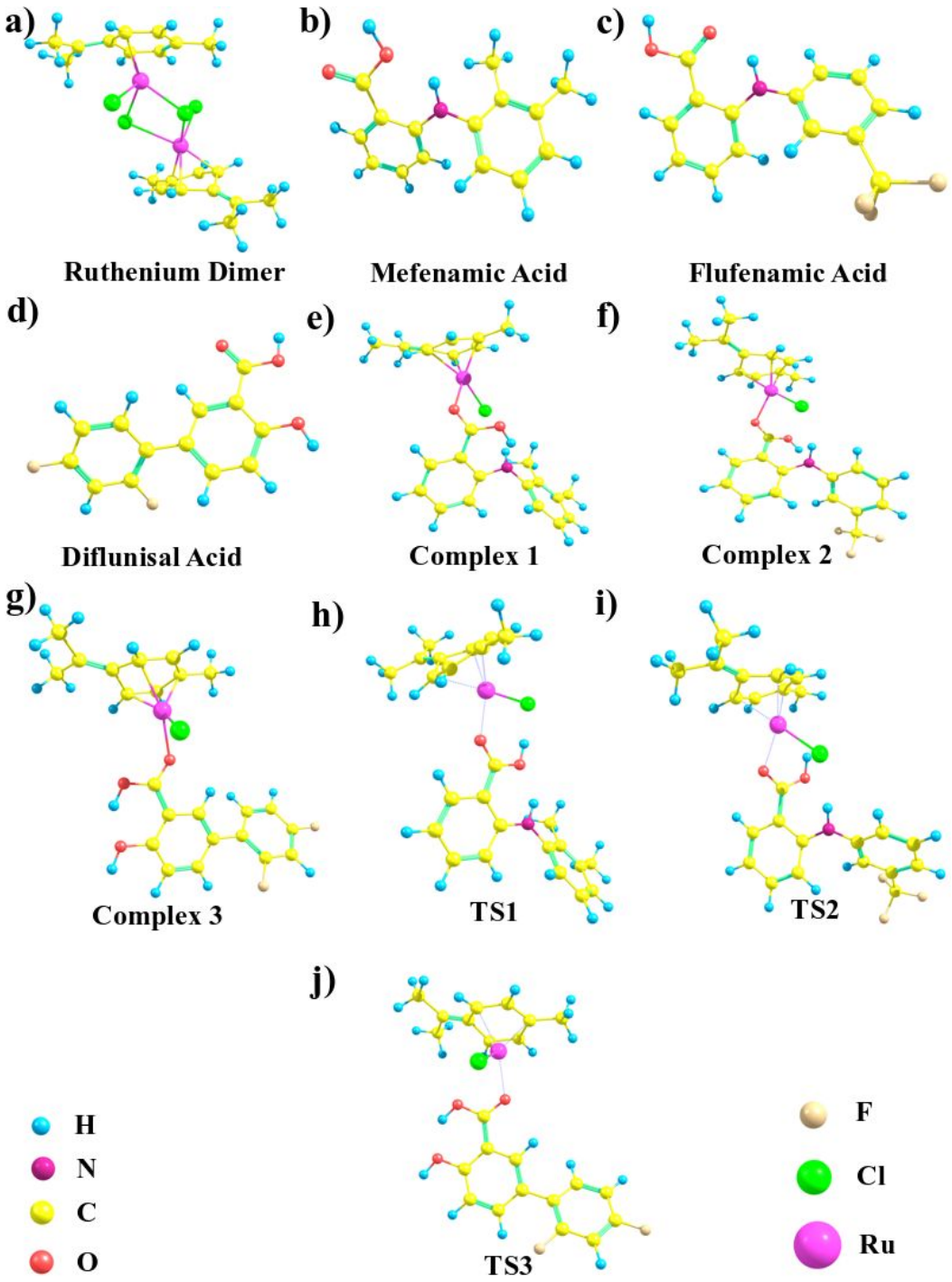

Figure 6: The equilibrium geometries of (a) ruthenium dimer, (b) mefenamic acid, (c) flufenamic acid, (d) diflunisal, (e) complex **1**, (f) complex **2**, (g) complex **3**, (h) transition state 1 (**TS1**: between the first adduct **A1** and complex **1** as a first product), (i) transition state 2 (**TS2**: between the second adduct **A2** and complex **2** as a second product), and (j) transition state 3 (**TS3**: between the third adduct A3 and complex **3** as a third product) computed by density functional theory (DFT) method.

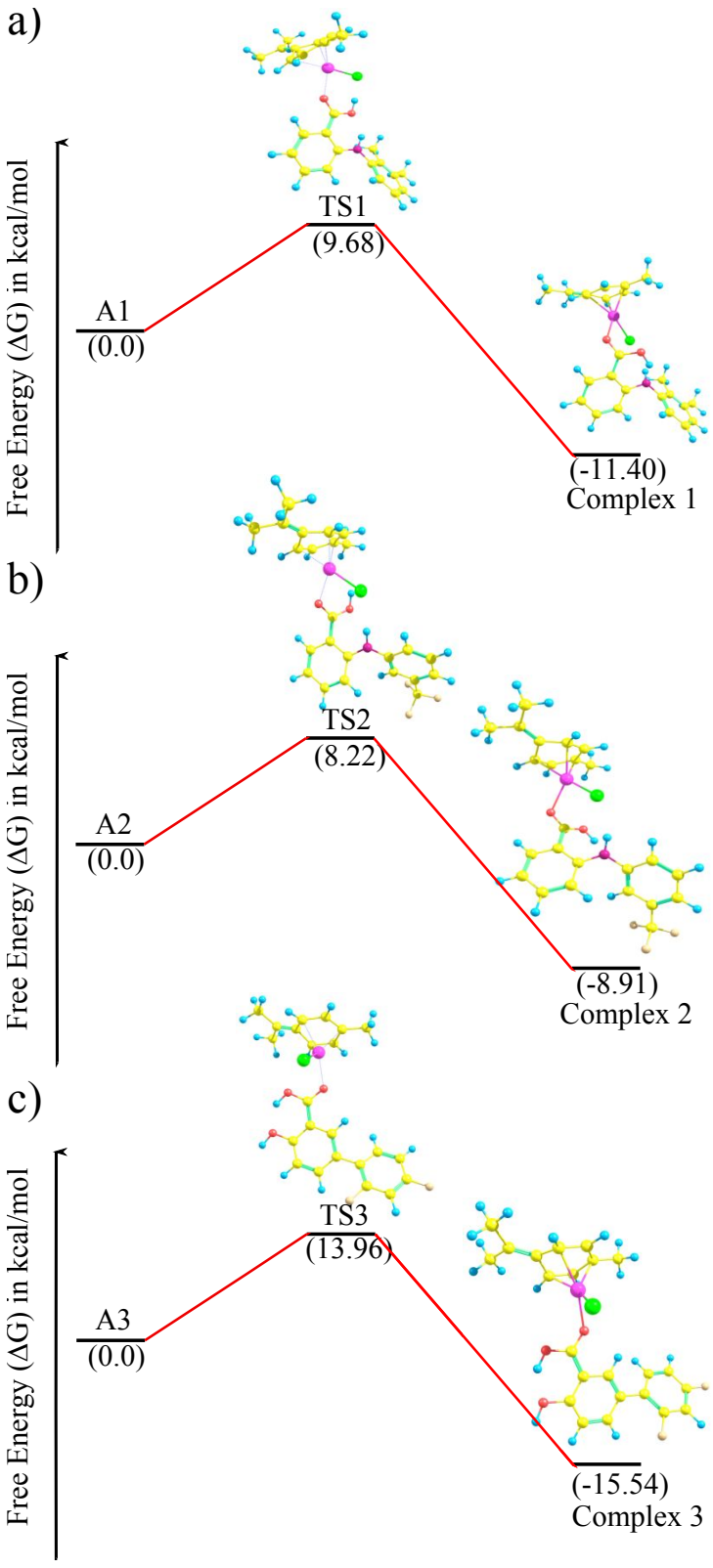

Figure 7: (a) The reaction pathway of the ruthenium dimer and mefenamic acid with the adduct **A1**, **TS1** and complex **1**; (b) the reaction pathway of the ruthenium dimer and flufenamic acid with the adduct **A2**, **TS2** and complex **2**; (c) the reaction pathway of the ruthenium dimer and diflunisal with the adduct **A3**, **TS3** and complex **3.**

In vitro cytotoxicity assay

The anticancer activity of free NSAIDs and complexes **1-3** was evaluated against three cancer cell lines *viz*. Human NSCLC cells (A549), breast carcinoma cells (MCF7), human cervical cancer (HeLa), and human embryonic kidney cells (HEK). In general complexes, **1-2** have shown considerable cytotoxicity against cancer cell lines having the IC_{50} values to the tune of μM concentration. However, all of them remain significantly non-cytotoxic against normal cell lines. All the relevant data of IC_{50} values for the different complexes are given in table **1** (Figure, S14-17). It is interesting to note that complex **1** is quite active against MCF7 although mildly cytotoxic against A549 and Hela. Complex **2** has shown considerable cytotoxicity against the MCF-7 cell line. Complex **3** remains non-toxic against all the cell lines. The DFT study also indicates that complex **3** is quite stable which might be the reason behind its non-cytotoxic behavior which might be reluctant towards reacting with biomolecules. Between complex **1** and **2**, the presence of two methyl groups in the mefenamic acid moiety might increase the lipophilicity of the complex **1.** This increased lipophilicity in complex **1** might help in the passive diffusion of the complex **1** into the cell and thus may act as the probable reason for higher cytotoxicity than complex **2**. Moreover, previous report shows that free mefenamic acid can show better anti-proliferative activity against different cancerous cell lines than flufenamic acid.[27]

Table 1. IC_{50} values of the synthesized complexes in human cancer cell lines (IC_{50} values are in μM and ± is a standard deviation)

Complexes	A549 (μM)	Hela (μM)	MCF7 (μM)	Hek293 (μM)
Complex **1**	35 ± 4	30 ± 5	10.6 ± 8	31 ± 5
Complex **2**	59 ± 3	52 ± 7	12 ± 3	64 ± 3
Complex **3**	72 ± 2	> 100	62 ± 4	63 ± 2
Doxurubicin	11 ± 6.2	12 ± 2	16 ± 4	14 ± 1

Interaction with DNA

DNA is considered to be a crucial molecular target for various drugs used in cancer therapeutics. Cisplatin and other platins have known to show cytotoxicity by binding to the DNA[28]. Thus evaluating the potential drug interaction with DNA may give us an imperative understanding of the action mechanism of the complexes for causing *in-vitro* cytotoxicity in cancer cells. Thus, to understand the plausible mechanism of the complexes as they show high to moderate cytotoxicity against certain cell lines, the DNA binding experiments have been carried out. Ethidium displacement has been utilized to enhance the understanding of the binding mechanism to the DNA. The ethidium bromide is an intercalating agent which in the unbound state is weakly fluorescent however when it interacts with DNA it gives orange fluorescence[29] which shows almost a 20 fold increase.

When complexes were added to the saturated solution of EtBr-DNA, it displaces EtBr from the EtBr-DNA complex which leads to the quenching of the fluorescence as unbound EtBr in the system increases. Thus, displacement of EtBr by the non-emissive complexes from the EtBr-DNA complex leads to remarkable quenching in the fluorescence pattern which can be easily visualized in the spectra (Figure S18). Reduction in fluorescence intensities when the ruthenium complexes displace EtBr from the DNA can be visualized in all the spectra observed at wavelength 614 nm. Thus, the significant binding of the complexes at the DNA-interaction sites can be indirectly concluded[30]. The K_{SV} (Stern-Volmer constant) values of the complexes **1, 2,** and **3** are found to be 2.6×10^4 M^{-1}, 7.5×10^4 M^{-1}, and 1.5×10^4 M^{-1}, respectively, which were calculated by Stern-Volmer equation[31].

$$\mathbf{F_0/F = 1+K_q\,[Q]}$$

Where F_0 and F represent the emission intensities of the EtBr-DNA complex, before and after the addition of complexes sequentially, respectively. The K_q values were obtained from the plot generated from the Scatchard equation. The plot of log $[(F_0\text{-}F)/F]$ versus log[Q] furnished K_q data, which are 3.5×10^{10}, 1.2×10^{10}, and 2.4×10^9 $M^{-1}sec^{-1}$ for the complexes **1**, **2** and **3**, respectively (Figure S19). All the relevant data are compiled in table 2. The K_a values of all the complexes were found to be comparable to the intercalator EB ($K_a = 1.23(\pm0.07) \times 10^5$ M^{-1})[32]. Reduced values for complex **3** for all the

parameters indicate its inability to bind DNA in a significant way which might be one of the reasons for its non-cytotoxic behavior.

Table 2. Summarized data of DNA binding

Complex	$K_{SV}(M^{-1})$	$K_q\,(M^{-1}S^{-1})$	$K_a\,(M^{-1})$	n
1	2.6×10^4	3.5×10^{10}	8.7×10^4	1.55
2	7.5×10^4	1.2×10^{10}	9×10^4	1.00
3	1.5×10^4	2.4×10^9	9×10^1	0.66

Interaction with proteins

Albumins are present in abundance in blood plasma which generally binds the prospective drug molecules, thus also play a crucial role in drug delivery system[33]. As most of the albumins are fluorescent in nature it has been considered that it is mostly caused by tyrosine, phenylalanine, and tryptophan residues in the protein. The interaction between protein and drug molecules is generally studied through the emission quenching of serum albumin. The fluorescence has been monitored by titrating with different concentrations of complexes (0-50 μM) to the BSA solution (1 μM) (Figure S20-S21). Protein binding is further evaluated by the Stern-Volmer equation[34], based on the bimolecular quenching rate constant and average time of fluorophore. The Stern-Volmer quenching equation is given by,

$$\mathbf{F_0/F = 1 + K_q\tau_0\,[Q] = 1 + K_{sv}[Q]}$$

Where F and F_0 represent tryptophan fluorescence intensity of serum albumin in the presence and absence of complex (quencher), [Q] concentration of the complex, τ_0 is the average life of the fluorophore in the absence of the complexes. The plot between log [F_0-F] versus log[Q] provides the information of two way quenching one by complexation and another by collision (Figure S22-S23). The K_{sv} and K_q values of the complexes are found to be in the range of 10^4 M^{-1} and 10^{12} $M^{-1}sec^{-1}$ respectively, which reveals the static quenching and strong binding between BSA and different

complexes. A similar trend can be also observed in HSA binding. There is a significant decrement in fluorescence intensity on the addition of the complexes that have been observed which determines the ground-state complex stability. Number of binding sites (n) and binding constant (K_a) were estimated through Scatchard equation[35] which is given by,

$$\mathbf{log[(F_0-F)/F] = logK_a + nlog[Q]}$$

Where, the binding sites and binding constants were determined by the plot of $log[(F_0-F)/F]$ versus log [Q] where the values of binding sites are found to be around 1. All the data are given in table 3.

Table 3. Summarized data of BSA and HSA binding.

Complex System	K_{SV} (M^{-1})	K_q ($M^{-1}S^{-1}$)	K_a (M^{-1})	n
1 with BSA	7.5×10^5	1.2×10^{10}	4×10^5	1.16
2 with BSA	1.5×10^5	2.5×10^{10}	2.7×10^5	1.30
3 with BSA	8×10^4	1.3×10^{10}	1.3×10^3	0.79
1 with HSA	2.8×10^5	4.5×10^{10}	6.4×10^5	1.31
2 with HSA	3.1×10^5	5.4×10^{10}	3.7×10^5	1.22
3 with HSA	1.4×10^5	2.4×10^{10}	3.5×10^4	1.07

Hoechst staining and Hoechst /PI staining

It is expected that the factor which acts behind the cell death on treatment with different ruthenium complexes is apoptosis where morphological changes in the nuclei, bi- or multi-nucleation, cytoplasmic blebbing, nuclear swelling, chromatin fragmentation and condensation should be explored as the significant characteristics of apoptotic cells and this can be determined by Hoechst staining[36]. So, the Hoechst staining experiment was carried out in MCF7 cells with IC_{50} values of complexes **1** and **2** and changes in the morphology were observed in the images captured with the help of confocal microscopy and presented in Figure 6. The normal cells are evenly and lightly stained however the cells treated with

complexes **1**, **2,** and positive control can be observed with multi-nucleation, condensed nuclei, and chromatin fragmentation.

To further explore the morphological changes that occurred due to probable apoptosis, Hoechst/PI staining was performed. Hoechst stain is cell-permeant to both live and dead cells whereas PI stain is impermeable to live cells[37]. On treating the cells with complexes **1**, **2** and positive control, changes can be observed evidently in the confocal microscope, where Hoechst stained cells show condensed and fragmented nuclei with the increased number of red fluorescence, whereas normal cells show uniformly lightly stained Hoechst blue fluorescence with very few red fluorescences as shown in Figure 8. The damaged cells are stained with PI which determines both late apoptotic and necrotic cells. The cells with vivid morphological changes and condensed chromatin and shrunk cells are contemplated as apoptotic cells, whereas the cells stained with PI indicates the dead cells[38]. In Figure 9 it can be easily visualized that there is a significant increase in the red fluorescence due to PI staining on the treatment of cells with complexes **1** and **2**, thus confirming the changes in morphology are in association with the plausible apoptosis. It also correlates with the anti-proliferative effects of the complexes which were determined by cell cytotoxicity assay.

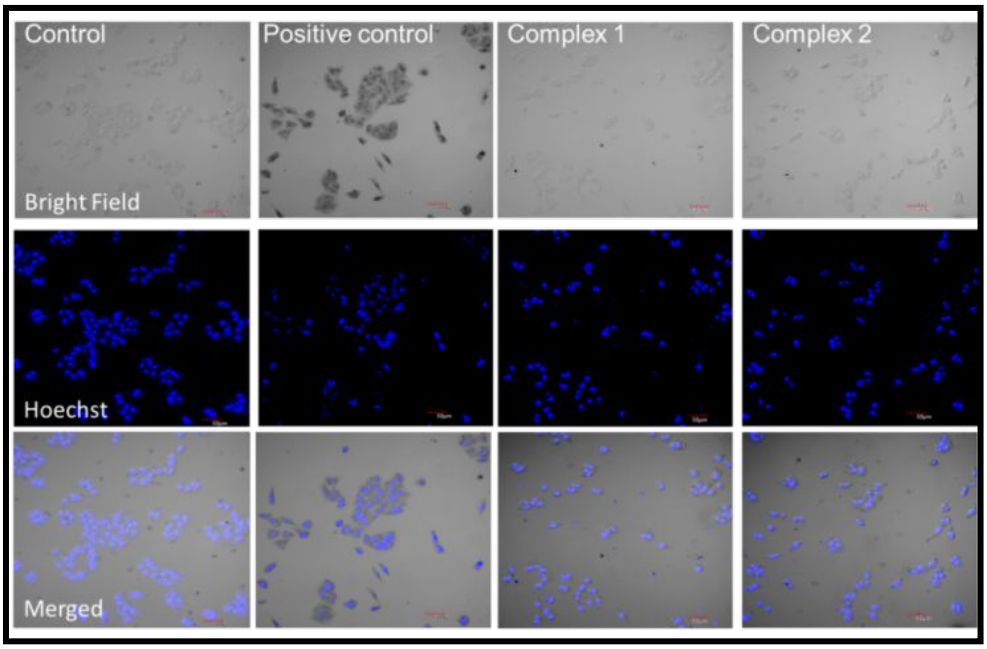

Figure 8. Hoechst staining of MCF7 cells, control, treatment of cells with complex **1**, treatment of cells with complex **2**, cells treated with 5-fluorouracil as a positive control.

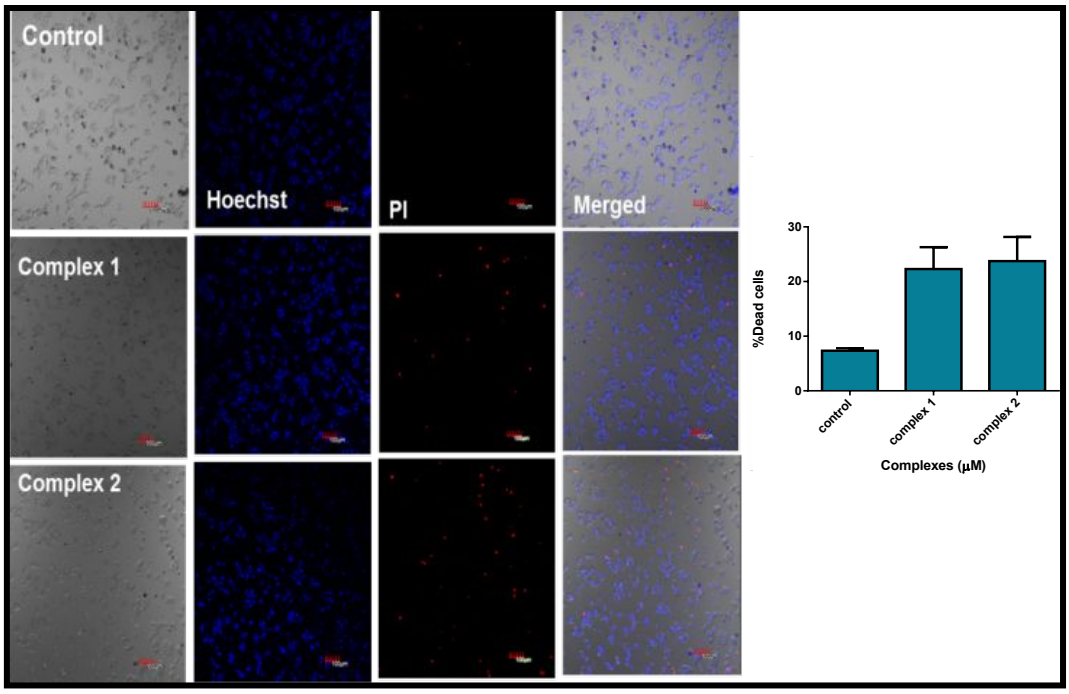

Figure 9. Hoechst and PI staining of MCF7 cells, control, treatment of cells with complex **1**, treatment of cells with complex **2**.

Cell migration assay

To further deduce the complexes **1** and **2** effects on cell migration, wound healing assay has been performed. Cell migration is characteristic of cancer cell invasion into the surrounding tissues[39]. This can be associated with several genes responsible for cell invasion, which can be potential targets for anti-metastatic drugs[40]. Wound closure activity gets significantly affected in the treatment of cells with IC_{50} concentration of complexes **1** and **2** as it can be seen from the Figure 10 that approximately 40% of the wounded area is yet to be covered in comparison with the control, thus depicting a substantial suppression of cell migration ability of complexes **1** and **2**.

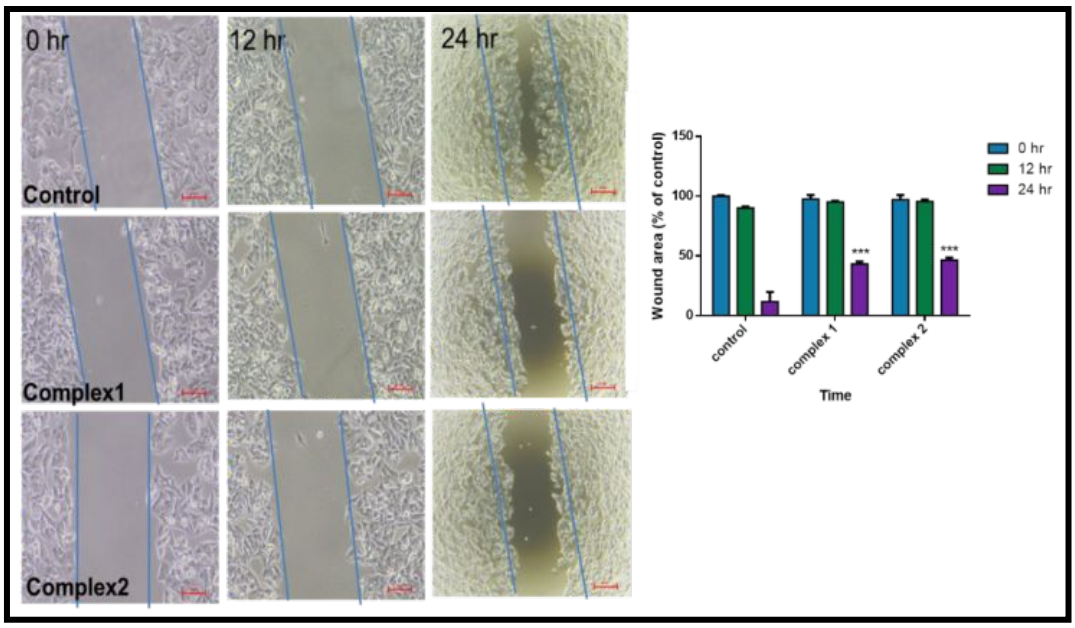

Figure 10. Cell migration assay in MCF7 cells, control, treatment of cells with complex **1**, treatment of cells with complex **2**.

Cell cycle analysis

Cell cycle ensures DNA duplication, and cell division thus is tightly regulated at various stages and by various proteins and pathways. However, concerning cancer cells, the cell cycle gets dysregulated[41]. Also, often the cause of cell growth inhibition in cell cycle arrest and this cell cycle arrest leads to apoptosis[42]. Many ruthenium complexes are found to show anticancer properties[43], which can be explored further by exploring their efficacy to arrest the cell cycle, thus inhibiting cells for proliferation.

To ascertain the contribution of cell cycle arrest in anti-proliferative activity, cell cycle distribution was analyzed using FACS analysis. The data show a significant increase of approximately (34.65% and 33.51%) in cell population G2/M phase when the cells are treated with complexes **1** and **2** respectively in comparison with the control (24.6%) (Figure 11). This implies that both the complexes are affecting the G2/M phase which in accordance with the previously reported data also observed in other half-sandwich Ru(II) and Ir(II) complexes[44].

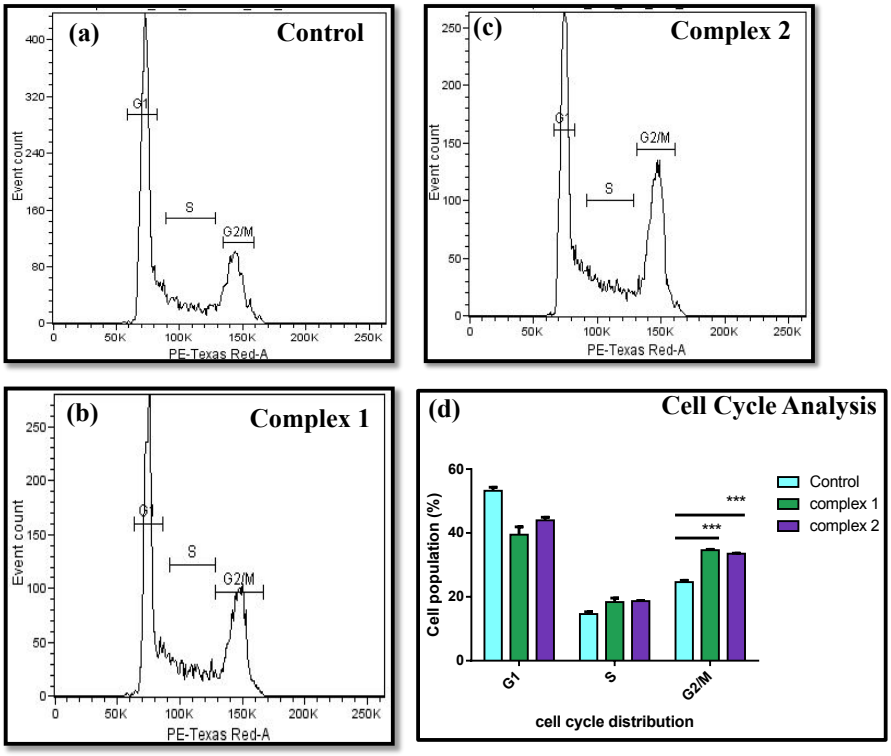

Figure 11. Cell cycle analysis on MCF-7 cell line, control(a), on treatment with IC_{50} concentration of Complex **1** (b), complex **2** (c) respectively for 4 hrs.(d) histogram depicting the % cell population distribution in cell cycle phase.

Modulation of apoptotic makers

Apoptosis is a programmed, well-regulated cellular phenomenon for eliminating undesired cells and maintaining homeostasis in the cells. Mitochondrial pathway-related apoptosis is dependent on the Bcl2 family which comprises both pro-apoptotic (Bax, Bak, and bok proteins) and anti-apoptotic protein (Bcl2, Bcl-XL, Mcl-1, Bcl-W, and A1)[45]. Bcl2 increased expression is a compelling indicator of cancer progression, thus its downregulation is expected by any proposed anticancer agents. Also, caspase-3 is regulated by both intrinsic (mitochondrial) and extrinsic signaling (death receptor) pathways of apoptosis[46]. Caspase-3 is also known as executioner protein which leads to the cleavage of various other proteins leading to gain and loss of function of the specific proteins, thus rendering apoptosis[47]. Here, our finding demonstrates a slight and significant decrease in Bcl2 gene expression along with the slight and significant increase in caspase 3 gene expression by complex **1** and **2** respectively. However, no

significant change in death receptor pathways related genes was visible, (Figure 12, S24) indicating probable no significant role of the extrinsic pathway in cell death.

Cell cycle arrest is a significant mechanism of cell death. The p53 and p21 proteins are important regulators of the cell cycle.[48] Thus, investigating the modulation in gene expression level may give cues related to other pathways involved in the cell death process. However, no such changes in gene expression were found, indicating a p53 and p21 independent cell death mechanism. Since no significant gene expression change can be observed in Bcl2, caspase 3, Fas, Fadd, p53, and p21 by treatment of complex **1**, hence, it implies mitochondrial independent pathway. Moreover, a significant decrease in Bcl2 expression and increase in caspase 3 gene expression was observed, but, no significant change was noticed in Fadd, Fas, p53, and p21, thus asserting the role of mitochondrial pathway in cell death by complex **2**.

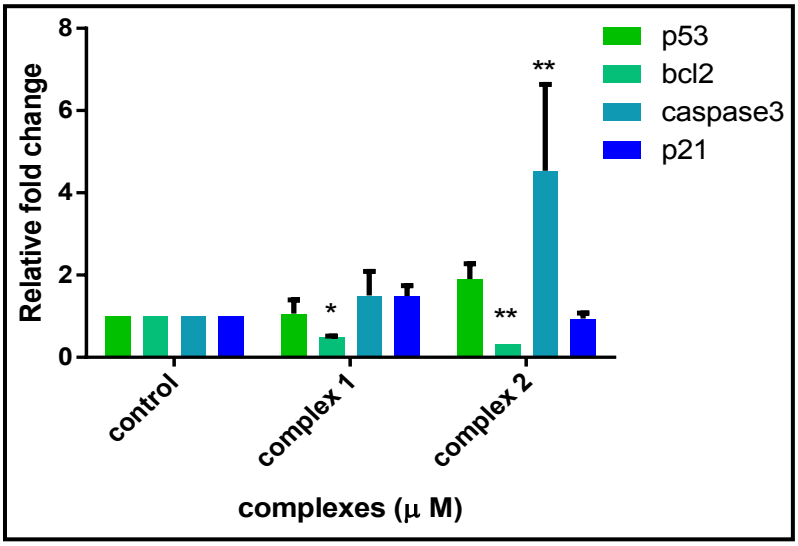

Figure 12. gene expression on the MCF-7 cell line, on treatment with IC_{50} concentration of Complex **1**, and complex **2** respectively.

CONCLUSION

Three new ruthenium NSAIDs complexes were made whose characterization was done through NMR, Mass, and IR. DFT calculations also reveal that all the proposed structures **1-3** are stable, and the computed reaction pathways with the barrier of the three transition states formed during the subject

reaction are in reasonable accordance with our experimental observation. Along with biological studies like protein and DNA binding studies, an attempt to find a probable mechanism of anticancer activities through Hoechst and dual staining is done. It was found that these complexes show anticancer properties through apoptosis which was confirmed by Hoechst PI staining. Through Cell cycle analysis it was depicted that there was a prominent increase in the G2/M phase which determines that the G2/M phase arrest might have induced the cell death by complex **1** and **2** respectively. The gene expression level of Bcl2 was prominently decreased and a noticeable increase in caspase3 was found on the treatment of cells with complex **2** indicating the mitochondrial-dependent pathway apoptosis.

EXPERIMENTAL SECTION

Material and methods

All the reagents were commercially available and utilized as received without any further purification. Flufenemic acid and diflunisal were purchased from Chempure (P) Ltd., 5 Fluorouracil, and Mefenamic acid were purchased from TCI chemicals. The rest of all the reagents were purchased from Merck Chemicals. Milli-Q water was utilized for recording NMR spectra at ambient temperature and DMSO-d_6 was used as a solvent for it. Hoechst PI stain and Cell cycle analysis quantification were done with the help of confocal microscope Fluoview FV100 (OLYMPUS, Tokyo, Japan) and LSR FORTEZZA (BD Biosciences) respectively. RT-PCR was carried out with applied biosystems 7300/7500. All the details of instruments used in the experiments are described well in the previous paper.[49]

Synthesis of [Ru(η^6-*p*-cymene)(mef)Cl] (Complex 1)

A solution of [Ru(η^6-*p*-cymene)Cl_2]$_2$ (0.1 g, 0.16 mol) prepared in dichloromethane (DCM, 50 mL) has been added in a dropwise manner to a methanolic solution (10 mL) of the potassium salt of mefenamic acid (0.09 g, 0.33 mmol), and stirred at room temperature for overnight. The resulting black colored solution was evaporated to dryness by the *in vacuo* and extracted with DCM (3 × 10 mL) and the extract

was further dried *in vacuo*. It was further washed with hexane and diethyl ether to obtain dark green colored powder which has been further recrystallized from DCM.

^{1}H NMR (400MHz, 298 K, $CDCl_3$) δ: 1.41 [(d, 6H, Ca, C*H*$_3$ of $(CH_3)_2CH$ (*p*-Cymene)], 2.14 [(S, 3H, Cc, C*H*$_3$(*p*-Cymene)], 2.32 [(S, 3H, Co)], 2.38 [(S, 3H, Cn)], 2.99 [m, 1H, Cb, C***H***$(CH_3)_2$ (*p*-Cymene)], 5.48 [(d, 2H, Ce, (*p*-cymene)], 5.71 [(d, 2H ,Cd, (*p*-cymene)], 6.59 [(d, 2H, Cg, Cm)] 6.62 [(t, 1H, Ch)], 6.99 (d, 2H ,Ck, Ci)], 7.08 (t, 1H, Cl)], 7.82 [(d, 1H, Cf)], 8.86 [(S, 1H, Cj], ^{13}C NMR (100MHz, $CDCl_3$) δ: 175.11 [Cj], 148.43 [Cp], 138.93 [Cq],138.06 [Cn], 133.89 [Cu], 132.40 [Cl], 131.21 [Cv], 128.98 [Ct], 126.55 [Cs], 125.83 [Cr], 123.21 [Cm], 116.06 [Co], 113.34 [Ck], 100.05 [Cg, CH of C_6H_4 (*p*-cymene)], 94.24 [Ci, CH of C_6H_4 (*p*-cymene)], 81.31 [Ch, CH of C_6H_4 (*p*-cymene)], 80.55 [Cf, CH of C_6H_4 (*p*-cymene)], 78.99 [Cd, CH of C_6H_4 (*p*-cymene)], 77.99 [Ce, CH of C_6H_4 (*p*-cymene)], 31.64 [Cb,*CH*$(CH_3)_2$], 22.49 [Ca,CH(*CH*$_3$)$_2$, (*p*-cymene)], 20.61 [*C*H$_3$, (*p*-cymene),Cc], 18.89 [Cw], 14.11 [Cx]. Elemental analysis for $C_{26}H_{31}ClNO_2Ru$ Calculated: C, 59.36; H,5.94; N,2.66. Found: C, 59.40; H,5.80 N,2.72. ESI-MS (+ve mode): [Ru(η^6-*p*-cymene)(mef)Cl+K]$^+$: 550 (*m/z*), yield :75%

Synthesis of [Ru(η^6-*p*-cymene)(flu)Cl] (Complex 2)

A methanolic solution (10 mL) of the potassium salt of flufenemic acid (0.1 g, 0.33 mmol) was added dropwise to the solution of $[Ru(\eta^6\text{-}p\text{-cymene})Cl_2]_2$ (0.1 g, 0.16 mol) dissolved in DCM (50 mL) and was kept for stirring for overnight at room temperature. The obtained green colored solution was dried *in vacuo*. Further extraction with dichloromethane and similar work up like the previous complex furnished complex **2**, resulting in the dark blue colored complex.

^{1}H NMR (400.13 MHz, 298 K, $CDCl_3$) δ: 1.41 [(d, 6H, Ca, C*H*$_3$ of $(CH_3)_2CH$ (*p*-Cymene)], 2.39 [(S, 3H, Cc, C*H*$_3$ (*p*-Cymene)], 3.00 [(m, 1H, Cb, C*H*$(CH_3)_2$ (*p*-Cymene)], 5.49 [(d, 2H, Cd, (*p*-Cymene)], 5.72 [(d, 2H ,Ce, (*p*-Cymene)], 6.75 [(m, 2H, Cj, Cl)], 7.16 [(d, 2H,Ch, Ci)], 7.39 [(d, 2H, Ck, Cm)], 7.44 [(S, 1H, Cg)], 7.88 [(d, 1H, Cf)], 9.18 (S, 1H, Cn). ^{13}C NMR (100.61 MHz, $CDCl_3$) δ: 177.83 [Ch], 146.86 [Cn], 145.82 [Co], 142.08 [Cl], 133.97 [Cq], 131.67 [Cj], 129.82 [Cs], 128.98 [Cu], 128.08 [Ct], 125.45 [Cp], 124.31[Ck], 119.21 [Cr], 118.35 [Cm], 114.23 [Ci], 100.51 [Cd, CH of C_6H_4

(*p*-cymene)], 94.28 [Ce, CH of C_6H_4 (*p*-cymene)], 78.64 [Cf, CH of C_6H_4 (*p*-cymene)], 78.08 [Cg, CH of C_6H_4 (*p*-cymene)], 31.72 [Cb, *C*H$(CH_3)_2$, (*p*-cymene)], 22.42 [Ca, CH(*C*$H_3)_2$, (*p*-cymene)], 18.91 [Cc, *C*H_3 (*p*-cymene)]. Elemental analysis for $C_{26}H_{31}ClNO_2Ru$ Calculated: C, 53.05; H,4.63; N,2.47 Found: C, 53.25; H,4.75; N,2.30. ESI-MS (+ve mode): [Ru(η^6-*p*-cymene)(flu)]$^+$: 518 (*m/z*) yield: 70%

Synthesis of [Ru(η6-*p*-cymene)(dif)Cl] (Complex 3)

The methanolic solution of diflunisal potassium salt (0.09 g, 0.33 mmol) was prepared and added dropwise to the solution of [Ru(η^6-*p*-cymene)Cl_2]$_2$ (0.1 g, 0.16 mol) in DCM (50 mL) and the solution was kept for stirring at room temperature for overnight. A yellowish colored solution was obtained which was dried *in vacuo*. Similar work-up like above-mentioned complexes furnished a powdered light brown colored complex **3**.

^{1}H NMR(400.13 MHz, 298 K, $CDCl_3$) δ: 1.42 [(d, 6H, Ca, C*H*$_3$ of $(CH_3)_2$CH (*p*-Cymene)], 2.35 [(S, 3H, Cc, C*H*$_3$(*p*-Cymene)], 2.98 [(m, 1H, Cb, C***H***$(CH_3)_2$ (*p*-Cymene)], 5.54 [(d, 2H, Ce, (*p*-Cymene)], 5.75 [(d, 2H ,Cd, (*p*-Cymene)], 5.92 [(S, 1H of Ck)], 6.82 [(d, 2H ,Cf, Cj)], 6.93 [(d, 2H, Cg, Ci)], 7.48 [(S, 1H, Ch)], ^{13}C NMR (100.61 MHz, $CDCl_3$) δ: 179.95 [Ch], 160.73 [Cr], 160.16 [Cp], 158.41 [Cj], 139.22 [Ci], 134.62 [Ct], 131.01 [Cn], 130.76 [Cl], 128.92 [Cm], 125.23 [Co], 117.10 [Ck], 114.03 [Cs], 111.44 [Cq], 104.10 [Cg, *C*H of C_6H_4 (*p*-cymene)], 98.66 [Cf, *C*H of C_6H_4 (*p*-cymene)], 81.78 [Ce, *C*H of C_6H_4 (*p*-cymene)], 77.71 [Cd, *C*H of C_6H_4 (*p*-cymene)], 31.91 [Cb, *C*H$(CH_3)_2$ (*p*-cymene)], 29.64 [Ca, CH(*C*$H_3)_2$ (*p*-cymene)], 22.36 [Cc, *C*H_3 (*p*-cymene)]. Elemental analysis for Calculated $C_{26}H_{31}ClNO_2Ru$: C, 53.88; H, 4.52. Found: C, 53.65; H, 4.75. ESI-MS (+ve mode): [Ru(η^6-*p*-cymene)(dif)]$^+$: 519 (*m/z)* yield : 68%

Computational Details

The equilibrium geometries of the ruthenium dimer, ruthenium monomer, mefenamic acid, flufenamic acid, diflunisal as reactants, and their complexes as products including first-order saddle points i.e. transition states (TS), were obtained with the *Density Functional Theory* (DFT) B3LYP method.[50,51]

The 6-31+G* type of Gaussian basis sets were utilized for the H, C, O, N, F, Cl atoms, and LANL2DZ with the effective core potentials (ECPs) was used for the Ru to reduce the computational expense.[52] It has shown that by using an ECPs with the respective basis sets such as LANL2DZ for transition metals has become more advanced and popular in computational chemistry on transition metal-containing systems, while exhausting all-electrons basis sets for other non-transition-metal atoms.[53] DFT has been extensively applied to predicting accurate equilibrium structure or geometry, reaction energies, change of enthalpy (ΔH), relative Gibbs free energy (ΔG), and reaction barrier heights, and it is found that the DFT gives trustworthy energy barriers for chemical reaction mechanisms and chemical thermodynamics.[54,55] A harmonic vibrational analysis was performed at the optimized geometries and saddle points (transition states) by applying the same B3LYP DFT method to unveil the stationary points and TSs nature. There was no imaginary frequency in the ruthenium dimer, ruthenium monomer, mefenamic acid, flufenamic acid, diflunisal, and their complexes which indicates a minimum level in potential energy curves. In other hand, only one imaginary frequency was in the TSs which was later confirmed by further computations of intrinsic reaction coordinate (IRC). The IRC computations were performed to validate the transition state (TS) structures obtained by the B3LYP method.[56] The DFT method (here B3LYP) was utilized for geometry optimization because densities and energies obtained with this method are hardly affected by spin contamination in comparison with other approaches.[51,57–63] All the calculations were carried out using the general-purpose electronic structure quantum chemistry program suite Gaussian 16.[64]

Stability of complexes

Since the stock solutions of complexes **1**, **2,** and **3** were prepared in DMSO therefore all the biological studies were carried out with 1% DMSO solution in the media. As it becomes imperative to evaluate the complex stability in DMSO the stability of the complexes was evaluated through ^{1}H and ^{13}C NMR in DMSO-d_6 at a time interval of 0 h, 12 h, 24 h.

EtBr displacement assay

The interaction of complexes **1**, **2,** and **3** with CT-DNA (calf thymus DNA) was determined with the help of the Fluoromax-4p spectrofluorometer. Fluorescence was recorded in the absence of complexes and then sequentially with the increasing amount of complexes. A buffer solution of CT DNA furnished a ratio of 1.8:1 of UV absorbance at 260 and 280 nm which depicts that the CT DNA is considerably free from protein contamination. The final CT DNA concentration was evaluated through a spectrophotometer by monitoring the extinction coefficient (6600 $cm^{-1}M^{-1}$). Thus an aqueous solution of 27 μM concentration of CT DNA in 2 mL of the cuvette with path length 1 cm was prepared in Tris-HCl buffer with pH 7.4. 10 μL of the complex solution from the stock solution (5mM in DMSO) was added sequentially to the CT-DNA solution in the presence of EtBr. The fluorescence intensities of EtBr (20 μM) bound with DNA with increasing concentration of the complex (0-100 uM) was measured at the excitation wavelength of 540 nm and the changes in the emission intensities were measured at 614 nm.

Albumin binding studies

The binding interaction experiments of complex **1**, **2,** and **3** with BSA and HSA were performed by monitoring the fluorescence of Tryptophan with excitation at 295 nm and its emission peaks at 340 nm. The concentrated BSA and HSA stock solution was prepared using 50 [mM] Tris-HCl buffer which has been diluted suitably. This BSA or HSA protein solution of 10 μM strength was further titrated with the further addition of respective complexes in the range of 0 to 100 μM.

Cell culture

Breast carcinoma cells (MCF7), Human NSCLC cells (A549), human embryonic kidney cells (HEK), human cervical cancer (HeLa), were purchased from NCCS (National Centre for Cell Science), Pune. MCF-7, HeLa, and HEK cells were cultured in Dulbecco minimum essential medium (DMEM). The

growth and maintenance procedure of the cell lines and materials used were as per our previous publication.[19]

In vitro cytotoxicity assay

The cells were seeded in 96-well flat-bottomed culture plate in 100 µl cell suspension and were incubated overnight at 37 °C in a 5% CO_2 incubator for attachment. Complex treatment was done by making 5mM stock solution of the complexes **1**, **2** and **3** in DMSO and then this stock solution was further diluted to 160µg, 80 µg, 40 µg, 20 µg. After 24 h treatment, the MTT experiment was carried out as per our previous publication.[19]

Hoechst staining

Morphology of the cells was evaluated using Hoechst stain 33258. The 5×10^4 MCF-7 cells were placed in 6 well plates having a coverslip in each well and were incubated overnight in the CO_2 incubator for attachment. The cells were then treated with corresponding IC_{50} concentration of 5 fluorouracil (positive control), complexes **1** and **2** for 24 h and untreated cells were taken as control. From the stock solution of 5-fluorouracil (5 mM prepared in DMSO), a 20 µL solution was added into each well already having 2 mL of media. The fixation and staining of the cells were carried out as per our previous publication.[19]

Hoechst and PI staining

To further confirm the nucleus morphology Hoechst 33258 and PI staining were carried out. The 5×10^4 MCF-7 cells were placed on 6 well plates (Nest; USA). The cells were treated with corresponding IC_{50} concentration of the complexes **1** and **2** followed by incubation for 24 h. The cells were trypsinized and the Hoechst, PI stain were directly added to the cell suspension with a concentration of 5µg/ml and 3µg/ml respectively, followed by incubation for 60 min at 37° C and washing with PBS thrice. The fluorescence was viewed by the help of Fluoview FV100 (OLYMPUS, Tokyo, Japan) confocal

microscope using appropriate filters. (Hoechst 33258 and PI having excitation wavelength 378 nm, 535 nm and an emission wavelength of 457 nm, 617 nm respectively)

Cell migration assay

To analyze the effect of complexes **1** and **2** on cell migration, cells were placed in 6 well plates and kept for incubation until confluent. Fully confluent cells were then wounded with the help of a yellow tip and then treated with IC_{50} concentration of the complexes and then the pictures were taken at a time interval of 0 h, 12 h, 24 h with the help of an inverted microscope.

Cell cycle analysis

Cells were placed in 6 well plates and incubated with the complexes for 4 h, after which the cells were trypsinized and resuspended in ice-cold PBS buffer. A further experiment was carried out as per our previous publication.[19] The data were analyzed with the help of LSR Fortessa (BD Biosciences).

RT-PCR

MCF-7 cells were placed in 6 well plates and were allowed to adhere overnight. These cells were now treated for 24 h with IC_{50} values of complexes **1** and **2**. RNA isolation was carried out using trizol reagent by following the manufacture's protocol. 5µg of RNA was used for the formation of cDNA by the Takara cDNA synthesis kit. The RT-PCR was carried out using SYBER green applied biosystems. The thermocycler conditions were set at 95ºC for 10 min, 40 cycles of 95 ºC for 15 sec, 54ºC for 20 sec, 72ºC for 20 sec, 95ºC for 15 sec, 60ºC for 1 min. The expression levels were analyzed with the help of a $2^{-\Delta\Delta t}$ method. The primers used for expression analyses are as follows (Table 4).

Table 4. The primers used for expression analyses.

Primers	Forward primer	Reverse primer
GAPDH	5'CCTGACCTGCCGTCTAGAAA 3'	5'TGGGTGTCGCTGTTGAAGTC 3'

P53	5’AGCACTGTCCAACAACACCA 3’	5’CTTCAGGTGGCTGGAGTGAG 3’
Caspase 3	5’ACCAAAGATCATACATGGAAGCG3’	5’TTCCCTGAGGTTTGCTGCAT 3’
Bcl2	5’GGTGAACTGGGGGAGGATTG 3’	5’GCCCAGACTCACATCACCAA 3’
P21	5’GCGACTGTGATGCGCTAATG 3’	5’GAAGGTAGAGCTTGGGCAGG 3’

Statistical Analysis

Data were evaluated as ± SEM. Statistical comparisons were analyzed with the help of graph pad prism software version 6. The *t*-test and two-way ANOVA were utilized for comparing two or more groups. The data having $p < 0.05$ was contemplated as statistically significant.

ASSOCIATED CONTENT

Supporting Information

Spectroscopic data, Analytical data, Biomolecular Interaction data, CT-DNA interaction data, Stability data, Cytotoxicity data, and Gene expression data.

The Supporting Information is available free of charge on the ACS Publications website.

AUTHOR INFORMATION

Corresponding Author

**E-mail: suman@iiti.ac.in. Phone: +91 731 2438 735. Fax: +91731 2361 482.

ORCID

Suman Mukhopadhyay: 0000-0002-5314-891X

Present Addresses

†Indian Institute of Technology Indore, India

Notes

The authors declare no competing financial interest.

ACKNOWLEDGMENT

We are grateful for DST SERB India (project no. SR/S1/IC-43/2012) for financially supporting this project. C. S. thank the Council of Scientific and Industrial Research (CSIR) for her fellowship. We also acknowledge the SIC, IIT Indore for their support in performing analytical studies. Dr. Srimanta Pakhira acknowledges the Science and Engineering Research Board-Department of Science and Technology (SERB-DST), Government of India for providing his Early Career Research Award (ECRA) under the project number ECR/2018/000255, and the highly prestigious Ramanujan Faculty Fellowship under the scheme number SB/S2/RJN-067/2017.

ABBREVIATIONS

NSCLC, non-small-cell lung carcinoma; MCF7, breast carcinoma cells; HEK, human embryonic kidney cells; HeLa, human cervical cancer; NCCS, National Centre for Cell Science; RPMI, Roswell Park Memorial Institute; DMEM, Dulbecco minimum essential medium; FBS, fetal bovine serum; NAMI-A, [trans-tetrachloro(DMSO) (imidazole)ruthenate(III)]; KP1019, [trans-tetrachlorobis(1H-indazole)ruthenate(III)]; NKP-1339, sodium trans-tetrachloride bis(1H-indazole) ruthenate(III)]; NSAIDs, non-steroidal anti-inflammatory drugs; COX, cyclooxygenase; LOX, lipooxygenase; HETEs, hydroxyeicosatetraenoic acids; EGF ,epidermal growth factor; DCM, dichloromethane; CT-DNA, calf thymus DNA; MTT,[3-(4,5-Dimethylthiazol-2-yl)-2,5- diphenyltetrazolium bromide]; EtBr, ethidium bromide.RT-PCR [Reverse transcription-polymerase chain reaction]

REFERENCES

(1) Zeng, L.; Gupta, P.; Chen, Y.; Wang, E.; Ji, L.; Chao, H.; Chen, Z.-S. The Development of Anticancer Ruthenium(II) Complexes: From Single Molecule Compounds to Nanomaterials. *Chem. Soc. Rev.* **2017**, *46* (19), 5771–5804. https://doi.org/10.1039/C7CS00195A.

(2) Novakova, O.; Chen, H.; Vrana, O.; Rodger, A.; Sadler, P. J.; Brabec, V. DNA Interactions of Monofunctional Organometallic Ruthenium(II) Antitumor Complexes in Cell-Free Media. *Biochemistry* **2003**, *42* (39), 11544–11554. https://doi.org/10.1021/bi034933u.

(3) Kisova, A.; Zerzankova, L.; Habtemariam, A.; Sadler, P. J.; Brabec, V.; Kasparkova, J. Differences in the Cellular Response and Signaling Pathways between Cisplatin and Monodentate Organometallic Ru(II) Antitumor Complexes Containing a Terphenyl Ligand. *Mol. Pharmaceutics* **2011**, *8* (3), 949–957. https://doi.org/10.1021/mp200105d.

(4) Bergamo, A.; Sava, G. Ruthenium Anticancer Compounds: Myths and Realities of the Emerging Metal-Based Drugs. *Dalton Trans.* **2011**, *40* (31), 7817–7823. https://doi.org/10.1039/C0DT01816C.

(5) Antonarakis, E. S.; Emadi, A. Ruthenium-Based Chemotherapeutics: Are They Ready for Prime Time? *Cancer Chemother Pharmacol* **2010**, *66* (1), 1–9. https://doi.org/10.1007/s00280-010-1293-1.

(6) Lenis-Rojas, O. A.; Robalo, M. P.; Tomaz, A. I.; Carvalho, A.; Fernandes, A. R.; Marques, F.; Folgueira, M.; Yáñez, J.; Vázquez-García, D.; López Torres, M.; Fernández, A.; Fernández, J. J. RuII(p-Cymene) Compounds as Effective and Selective Anticancer Candidates with No Toxicity in Vivo. *Inorg. Chem.* **2018**, *57* (21), 13150–13166. https://doi.org/10.1021/acs.inorgchem.8b01270.

(7) Wongrakpanich, S.; Wongrakpanich, A.; Melhado, K.; Rangaswami, J. A Comprehensive Review of Non-Steroidal Anti-Inflammatory Drug Use in The Elderly. *Aging Dis* **2018**, *9* (1), 143–150. https://doi.org/10.14336/AD.2017.0306.

(8) Phillips, W.; Currier, B. Analgesic Pharmacology: II. Specific Analgesics. *Journal of the American Academy of Orthopaedic Surgeons* **2004**, *12* (4), 221–233.

(9) Pannunzio, A.; Coluccia, M. Cyclooxygenase-1 (COX-1) and COX-1 Inhibitors in Cancer: A Review of Oncology and Medicinal Chemistry Literature. *Pharmaceuticals (Basel)* **2018**, *11* (4), 101. https://doi.org/10.3390/ph11040101.

(10) Luci, D. K.; Jameson, J. B.; Yasgar, A.; Diaz, G.; Joshi, N.; Kantz, A.; Markham, K.; Perry, S.; Kuhn, N.; Yeung, J.; Kerns, E. H.; Schultz, L.; Holinstat, M.; Nadler, J. L.; Taylor-Fishwick, D. A.; Jadhav, A.; Simeonov, A.; Holman, T. R.; Maloney, D. J. Synthesis and Structure–Activity

Relationship Studies of 4-((2-Hydroxy-3-Methoxybenzyl)Amino)Benzenesulfonamide Derivatives as Potent and Selective Inhibitors of 12-Lipoxygenase. *J Med Chem* **2014**, *57* (2), 495–506. https://doi.org/10.1021/jm4016476.

(11) Zhang, Y.; Tortorella, M. D.; Liao, J.; Qin, X.; Chen, T.; Luo, J.; Guan, J.; Talley, J. J.; Tu, Z. Synthesis and Evaluation of Novel Erlotinib–NSAID Conjugates as More Comprehensive Anticancer Agents. *ACS Med Chem Lett* **2015**, *6* (10), 1086–1090. https://doi.org/10.1021/acsmedchemlett.5b00286.

(12) Basu, U.; Banik, B.; Wen, R.; Pathak, R. K.; Dhar, S. The Platin-X Series: Activation, Targeting, and Delivery. *Dalton Trans.* **2016**, *45* (33), 12992–13004. https://doi.org/10.1039/C6DT01738J.

(13) Tatematsu, Y.; Hayashi, H.; Taguchi, R.; Fujita, H.; Yamamoto, A.; Ohkura, K. Effect of *N*-Phenylanthranilic Acid Scaffold Nonsteroidal Anti-Inflammatory Drugs on the Mitochondrial Permeability Transition. *Biological and Pharmaceutical Bulletin* **2016**, *39* (2), 278–284. https://doi.org/10.1248/bpb.b15-00717.

(14) Mandal, P.; Kundu, B. K.; Vyas, K.; Sabu, V.; Helen, A.; Dhankhar, S. S.; Nagaraja, C. M.; Bhattacherjee, D.; Bhabak, K. P.; Mukhopadhyay, S. Ruthenium(II) Arene NSAID Complexes: Inhibition of Cyclooxygenase and Antiproliferative Activity against Cancer Cell Lines. *Dalton Trans.* **2018**, *47* (2), 517–527. https://doi.org/10.1039/C7DT03637J.

(15) Becke, A. D. Density-functional Thermochemistry. III. The Role of Exact Exchange. *J. Chem. Phys.* **1993**, *98* (7), 5648–5652. https://doi.org/10.1063/1.464913.

(16) Sheeba, M. M.; Muthu Tamizh, M.; Farrugia, L. J.; Endo, A.; Karvembu, R. Chiral (H6-p-Cymene)Ruthenium(II) Complexes Containing Monodentate Acylthiourea Ligands for Efficient Asymmetric Transfer Hydrogenation of Ketones. *Organometallics* **2014**, *33* (2), 540–550. https://doi.org/10.1021/om4010548.

(17) Biancalana, L.; Batchelor, L. K.; Funaioli, T.; Zacchini, S.; Bortoluzzi, M.; Pampaloni, G.; Dyson, P. J.; Marchetti, F. α-Diimines as Versatile, Derivatizable Ligands in Ruthenium(II) p-

Cymene Anticancer Complexes. *Inorg. Chem.* **2018**, *57* (11), 6669–6685. https://doi.org/10.1021/acs.inorgchem.8b00882.

(18) Tsiliou, S.; Kefala, L.-A.; Perdih, F.; Turel, I.; Kessissoglou, D. P.; Psomas, G. Cobalt(II) Complexes with Non-Steroidal Anti-Inflammatory Drug Tolfenamic Acid: Structure and Biological Evaluation. *European Journal of Medicinal Chemistry* **2012**, *48*, 132–142. https://doi.org/10.1016/j.ejmech.2011.12.004.

(19) Malviya, N.; Sonkar, C.; Ganguly, R.; Bhattacherjee, D.; Bhabak, K. P.; Mukhopadhyay, S. Novel Approach to Generate a Self-Deliverable Ru(II)-Based Anticancer Agent in the Self-Reacting Confined Gel Space. *ACS Appl. Mater. Interfaces* **2019**, *11* (50), 47606–47618. https://doi.org/10.1021/acsami.9b17075.

(20) Kumar, P.; Swagatika, S.; Dasari, S.; Tomar, R. S.; Patra, A. K. Modulation of Ruthenium Anticancer Drugs Analogs with Tolfenamic Acid: Reactivity, Biological Interactions and Growth Inhibition of Yeast Cell. *Journal of Inorganic Biochemistry* **2019**, *199*, 110769. https://doi.org/10.1016/j.jinorgbio.2019.110769.

(21) Aman, F.; Hanif, M.; Siddiqui, W. A.; Ashraf, A.; Filak, L. K.; Reynisson, J.; Söhnel, T.; Jamieson, S. M. F.; Hartinger, C. G. Anticancer Ruthenium(H6-p-Cymene) Complexes of Nonsteroidal Anti-Inflammatory Drug Derivatives. *Organometallics* **2014**, *33* (19), 5546–5553. https://doi.org/10.1021/om500825h.

(22) Hashemipour, M. A.; Mehrabizadeh Honarmand, H.; Falsafi, F.; Tahmasebi Arashlo, M.; Rajabalian, S.; Gandjalikhan Nassab, S. A. H. In Vitro Cytotoxic Effects of Celecoxib, Mefenamic Acid, Aspirin and Indometacin on Several Cells Lines. *J Dent (Shiraz)* **2016**, *17* (3), 219–225.

(23) Calimano, E.; Don Tilley, T. Synthesis and Reactivity of Rhodium and Iridium Alkene , Alkyl and Silyl Complexes Supported by a Phenyl -Substituted PNP Pincer Ligand. *Dalton Transactions* **2010**, *39* (39), 9250–9263. https://doi.org/10.1039/B925856F.

(24) Hawksworth, E. L.; Andrews, P. C.; Lie, W.; Lai, B.; Dillon, C. T. Biological Evaluation of Bismuth Non-Steroidal Anti-Inflammatory Drugs (BiNSAIDs): Stability, Toxicity and Uptake in HCT-8 Colon Cancer Cells. *Journal of Inorganic Biochemistry* **2014**, *135*, 28–39. https://doi.org/10.1016/j.jinorgbio.2014.02.012.

(25) Thota, S.; Rodrigues, D. A.; Crans, D. C.; Barreiro, E. J. Ru(II) Compounds: Next-Generation Anticancer Metallotherapeutics? *J. Med. Chem.* **2018**, *61* (14), 5805–5821. https://doi.org/10.1021/acs.jmedchem.7b01689.

(26) Tadić, A.; Poljarević, J.; Krstić, M.; Kajzerberger, M.; Aranđelović, S.; Radulović, S.; Kakoulidou, C.; Papadopoulos, A. N.; Psomas, G.; Grgurić-Šipka, S. Ruthenium–Arene Complexes with NSAIDs: Synthesis, Characterization and Bioactivity. *New J. Chem.* **2018**, *42* (4), 3001–3019. https://doi.org/10.1039/C7NJ04416J.

(27) Soriano-Hernandez, A. D.; Madrigal-Pérez, D.; Galvan-Salazar, H. R.; Martinez-Fierro, M. L.; Valdez-Velazquez, L. L.; Espinoza-Gómez, F.; Vazquez-Vuelvas, O. F.; Olmedo-Buenrostro, B. A.; Guzman-Esquivel, J.; Rodriguez-Sanchez, I. P.; Lara-Esqueda, A.; Montes-Galindo, D. A.; Delgado-Enciso, I. Anti-inflammatory Drugs and Uterine Cervical Cancer Cells: Antineoplastic Effect of Meclofenamic Acid. *Oncology Letters* **2015**, *10* (4), 2574–2578. https://doi.org/10.3892/ol.2015.3580.

(28) Hurley, L. H. DNA and Its Associated Processes as Targets for Cancer Therapy. *Nature Reviews Cancer* **2002**, *2* (3), 188–200. https://doi.org/10.1038/nrc749.

(29) Mukhopadhyay, S.; Gupta, R. K.; Paitandi, R. P.; Rana, N. K.; Sharma, G.; Koch, B.; Rana, L. K.; Hundal, M. S.; Pandey, D. S. Synthesis, Structure, DNA/Protein Binding, and Anticancer Activity of Some Half-Sandwich Cyclometalated Rh(III) and Ir(III) Complexes. *Organometallics* **2015**, *34* (18), 4491–4506. https://doi.org/10.1021/acs.organomet.5b00475.

(30) Senthil Raja, D.; P. Bhuvanesh, N. S.; Natarajan, K. A Novel Water Soluble Ligand Bridged Cobalt(Ii) Coordination Polymer of 2-Oxo-1,2-Dihydroquinoline-3-Carbaldehyde (Isonicotinic) Hydrazone: Evaluation of the DNA Binding, Protein Interaction, Radical Scavenging and

Anticancer Activity. *Dalton Transactions* **2012**, *41* (15), 4365–4377. https://doi.org/10.1039/C2DT12274J.

(31) Jeyalakshmi, K.; Haribabu, J.; Balachandran, C.; Swaminathan, S.; Bhuvanesh, N. S. P.; Karvembu, R. Coordination Behavior of N,N′,N″-Trisubstituted Guanidine Ligands in Their Ru–Arene Complexes: Synthetic, DNA/Protein Binding, and Cytotoxic Studies. *Organometallics* **2019**, *38* (4), 753–770. https://doi.org/10.1021/acs.organomet.8b00702.

(32) Tsiliki, P.; Perdih, F.; Turel, I.; Psomas, G. Structure, DNA- and Albumin-Binding of the Manganese(II) Complex with the Non-Steroidal Antiinflammatory Drug Niflumic Acid. *Polyhedron* **2013**, *53*, 215–222. https://doi.org/10.1016/j.poly.2013.01.049.

(33) Dömötör, O.; Hartinger, C. G.; Bytzek, A. K.; Kiss, T.; Keppler, B. K.; Enyedy, E. A. Characterization of the Binding Sites of the Anticancer Ruthenium(III) Complexes KP1019 and KP1339 on Human Serum Albumin via Competition Studies. *J Biol Inorg Chem* **2013**, *18* (1), 9–17. https://doi.org/10.1007/s00775-012-0944-6.

(34) Jeyalakshmi, K.; Haribabu, J.; Balachandran, C.; Bhuvanesh, N. S. P.; Emi, N.; Karvembu, R. Synthesis of Ru(II)–Benzene Complexes Containing Aroylthiourea Ligands, and Their Binding with Biomolecules and in Vitro Cytotoxicity through Apoptosis. *New J. Chem.* **2017**, *41* (7), 2672–2686. https://doi.org/10.1039/C6NJ03099H.

(35) Raja, D. S.; Paramaguru, G.; Bhuvanesh, N. S. P.; Reibenspies, J. H.; Renganathan, R.; Natarajan, K. Effect of Terminal N-Substitution in 2-Oxo-1,2-Dihydroquinoline-3-Carbaldehyde Thiosemicarbazones on the Mode of Coordination, Structure, Interaction with Protein, Radical Scavenging and Cytotoxic Activity of Copper(II) Complexes. *Dalton Trans.* **2011**, *40* (17), 4548–4559. https://doi.org/10.1039/C0DT01657H.

(36) Yan, Y.; Su, X.; Liang, Y.; Zhang, J.; Shi, C.; Lu, Y.; Gu, L.; Fu, L. Emodin Azide Methyl Anthraquinone Derivative Triggers Mitochondrial-Dependent Cell Apoptosis Involving in Caspase-8-Mediated Bid Cleavage. *Mol Cancer Ther* **2008**, *7* (6), 1688–1697. https://doi.org/10.1158/1535-7163.MCT-07-2362.

(37) Molnár, J.; Frank, É.; Minorics, R.; Kádár, Z.; Ocsovszki, I.; Schönecker, B.; Wölfling, J.; Zupkó, I. A Click Approach to Novel D-Ring-Substituted 16α-Triazolylestrone Derivatives and Characterization of Their Antiproliferative Properties. *PLoS One* **2015**, *10* (2), e0118104. https://doi.org/10.1371/journal.pone.0118104.

(38) Minorics, R.; Szekeres, T.; Krupitza, G.; Saiko, P.; Giessrigl, B.; Wölfling, J.; Frank, É.; Zupkó, I. Antiproliferative Effects of Some Novel Synthetic Solanidine Analogs on HL-60 Human Leukemia Cells in Vitro. *Steroids* **2011**, *76* (1), 156–162. https://doi.org/10.1016/j.steroids.2010.10.006.

(39) Chambers, A. F.; Groom, A. C.; MacDonald, I. C. Dissemination and Growth of Cancer Cells in Metastatic Sites. *Nature Reviews Cancer* **2002**, *2* (8), 563–572. https://doi.org/10.1038/nrc865.

(40) Wang, W.; Goswami, S.; Lapidus, K.; Wells, A. L.; Wyckoff, J. B.; Sahai, E.; Singer, R. H.; Segall, J. E.; Condeelis, J. S. Identification and Testing of a Gene Expression Signature of Invasive Carcinoma Cells within Primary Mammary Tumors. *Cancer Res* **2004**, *64* (23), 8585–8594. https://doi.org/10.1158/0008-5472.CAN-04-1136.

(41) Pietenpol, J. A.; Stewart, Z. A. Cell Cycle Checkpoint Signaling:: Cell Cycle Arrest versus Apoptosis. *Toxicology* **2002**, *181–182*, 475–481. https://doi.org/10.1016/S0300-483X(02)00460-2.

(42) Pucci, B.; Kasten, M.; Giordano, A. Cell Cycle and Apoptosis. *Neoplasia* **2000**, *2* (4), 291–299.

(43) Yellol, G. S.; Donaire, A.; Yellol, J. G.; Vasylyeva, V.; Janiak, C.; Ruiz, J. On the Antitumor Properties of Novel Cyclometalated Benzimidazole Ru(II), Ir(III) and Rh(III) Complexes. *Chem. Commun.* **2013**, *49* (98), 11533–11535. https://doi.org/10.1039/C3CC46239K.

(44) Ma, W.; Zhang, S.; Tian, Z.; Xu, Z.; Zhang, Y.; Xia, X.; Chen, X.; Liu, Z. Potential Anticancer Agent for Selective Damage to Mitochondria or Lysosomes: Naphthalimide-Modified Fluorescent Biomarker Half-Sandwich Iridium (III) and Ruthenium (II) Complexes. *European Journal of Medicinal Chemistry* **2019**, *181*, 111599. https://doi.org/10.1016/j.ejmech.2019.111599.

(45) Pinton, P.; Giorgi, C.; Siviero, R.; Zecchini, E.; Rizzuto, R. Calcium and Apoptosis: ER-Mitochondria Ca2+ Transfer in the Control of Apoptosis. *Oncogene* **2008**, *27* (50), 6407–6418. https://doi.org/10.1038/onc.2008.308.

(46) Green, D. R.; Llambi, F. Cell Death Signaling. *Cold Spring Harb Perspect Biol* **2015**, *7* (12), a006080. https://doi.org/10.1101/cshperspect.a006080.

(47) Ghobrial, I. M.; Witzig, T. E.; Adjei, A. A. Targeting Apoptosis Pathways in Cancer Therapy. *CA: A Cancer Journal for Clinicians* **2005**, *55* (3), 178–194. https://doi.org/10.3322/canjclin.55.3.178.

(48) Lee, J.-M.; Kwon, H.; Jeong, H.; Lee, J. W.; Lee, S. Y.; Baek, S. J.; Surh, Y.-J. Inhibition of Lipid Peroxidation and Oxidative DNA Damage by Ganoderma Lucidum. *Phytotherapy Research* **2001**, *15* (3), 245–249. https://doi.org/10.1002/ptr.830.

(49) Das, M.; Kumar Kundu, B.; Tiwari, R.; Mandal, P.; Nayak, D.; Ganguly, R.; Mukhopadhyay, S. Investigation on Chemical Protease, Nuclease and Catecholase Activity of Two Copper Complexes with Flexidentate Schiff Base Ligands. *Inorganica Chimica Acta* **2018**, *469*, 111–122. https://doi.org/10.1016/j.ica.2017.09.013.

(50) Lee, C.; Yang, W.; Parr, R. G. Development of the Colle-Salvetti Correlation-Energy Formula into a Functional of the Electron Density. *Phys. Rev. B* **1988**, *37* (2), 785–789. https://doi.org/10.1103/PhysRevB.37.785.

(51) Pakhira, S. Rotational Dynamics of the Organic Bridging Linkers in Metal–Organic Frameworks and Their Substituent Effects on the Rotational Energy Barrier. *RSC Advances* **2019**, *9* (65), 38137–38147. https://doi.org/10.1039/C9RA01288E.

(52) Pritchard, B. P.; Altarawy, D.; Didier, B.; Gibson, T. D.; Windus, T. L. New Basis Set Exchange: An Open, Up-to-Date Resource for the Molecular Sciences Community. *J. Chem. Inf. Model.* **2019**, *59* (11), 4814–4820. https://doi.org/10.1021/acs.jcim.9b00725.

(53) Yang, Y.; Weaver, M. N.; Merz, K. M. Assessment of the "6-31+G** + LANL2DZ" Mixed Basis Set Coupled with Density Functional Theory Methods and the Effective Core Potential:

Prediction of Heats of Formation and Ionization Potentials for First-Row-Transition-Metal Complexes. *J. Phys. Chem. A* **2009**, *113* (36), 9843–9851. https://doi.org/10.1021/jp807643p.

(54) Pakhira, S.; Lengeling, B. S.; Olatunji-Ojo, O.; Caffarel, M.; Frenklach, M.; Lester, W. A. A Quantum Monte Carlo Study of the Reactions of CH with Acrolein. *J. Phys. Chem. A* **2015**, *119* (18), 4214–4223. https://doi.org/10.1021/acs.jpca.5b00919.

(55) S, P.; Ri, S.; O, O.-O.; M, F.; Jr, L. W. Quantum Monte Carlo Study of the Reactions of CH with Acrolein: Major and Minor Channels. *J Phys Chem A* **2016**, *120* (20), 3602–3612. https://doi.org/10.1021/acs.jpca.5b11527.

(56) Gonzalez, Carlos.; Schlegel, H. Bernhard. Reaction Path Following in Mass-Weighted Internal Coordinates. *J. Phys. Chem.* **1990**, *94* (14), 5523–5527. https://doi.org/10.1021/j100377a021.

(57) Baker, J.; Scheiner, A.; Andzelm, J. Spin Contamination in Density Functional Theory. *Chemical Physics Letters* **1993**, *216* (3), 380–388. https://doi.org/10.1016/0009-2614(93)90113-F.

(58) Montoya, A.; Truong, T. N.; Sarofim, A. F. Spin Contamination in Hartree−Fock and Density Functional Theory Wavefunctions in Modeling of Adsorption on Graphite. *J. Phys. Chem. A* **2000**, *104* (26), 6108–6110. https://doi.org/10.1021/jp000534m.

(59) Pople, J. A.; Gill, P. M. W.; Handy, N. C. Spin-Unrestricted Character of Kohn-Sham Orbitals for Open-Shell Systems. *International Journal of Quantum Chemistry* **1995**, *56* (4), 303–305. https://doi.org/10.1002/qua.560560414.

(60) Pakhira, S.; Sen, K.; Sahu, C.; Das, A. K. Performance of Dispersion-Corrected Double Hybrid Density Functional Theory: A Computational Study of OCS-Hydrocarbon van Der Waals Complexes. *J. Chem. Phys.* **2013**, *138* (16), 164319. https://doi.org/10.1063/1.4802247.

(61) Cioslowski, J.; Liu, G.; Martinov, M.; Piskorz, P.; Moncrieff, D. Energetics and Site Specificity of the Homolytic C−H Bond Cleavage in Benzenoid Hydrocarbons: An Ab Initio Electronic Structure Study. *J. Am. Chem. Soc.* **1996**, *118* (22), 5261–5264. https://doi.org/10.1021/ja9600439.

(62) Sinha, N.; Deshpande, I.; Pakhira, S. Substituents Effects of Organic Linkers on Rotational Energy Barriers in Metal-Organic Frameworks. *ChemistrySelect* **2019**, *4* (29), 8584–8592. https://doi.org/10.1002/slct.201901278.

(63) Pakhira, S.; Sahu, C.; Sen, K.; Das, A. K. Can Two T-Shaped Isomers of OCS–C2H2 van Der Waals Complex Exist? *Chemical Physics Letters* **2012**, *549*, 6–11. https://doi.org/10.1016/j.cplett.2012.08.043.

(64) Citation | Gaussian.com https://gaussian.com/citation/ (accessed Apr 27, 2020).

Table of Contents